

Enabling high giant magnetoresistance in ultrathin-free-layer spin valves

Sachli Abdizadeh,¹ Rachel E. Maizel,¹ Jing Zhao,² F. Marc Michel,^{2,3} and Satoru Emori^{1,3}

¹⁾Department of Physics, Virginia Tech, Blacksburg, Virginia 24061, USA

²⁾Department of Geosciences, Virginia Tech, Blacksburg, Virginia 24061, USA

³⁾Academy of Integrated Science, Virginia Tech, Blacksburg, Virginia 24061, USA

(*Electronic mail: sachli@vt.edu; semori@vt.edu)

(Dated: 30 December 2025)

Emerging spin-orbit-torque devices based on spin valves require an ultrathin (e.g., $\lesssim 2$ nm) magnetic free layer to maximize the torque per moment. However, reducing the free-layer thickness deteriorates the giant magnetoresistance (GMR) signal for electrical readout. Here, we demonstrate that the addition of a 1-nm Cu seed layer enables high GMR ratios of 5–7% at free-layer thicknesses of $\lesssim 2$ nm by promoting high-quality, textured growth of spin valves. Our work offers a pathway for engineering high-signal GMR readout in spin-orbit-torque digital memories and neuromorphic computers.

Spin valves, consisting of a “free layer” with a switchable magnetization and a “fixed layer” with a pinned magnetization, offer a promising platform for next-generation nanomagnetic devices driven by spin-orbit torques^{1,2}. In this device architecture, an in-plane electric current through the fixed layer produces an out-of-plane spin current^{3,4}, which exerts a torque on the magnetization in the free layer. This torque enables magnetic switching for digital memories⁵ or large-angle precession for oscillators⁶ in neuromorphic computing⁷. Furthermore, the giant magnetoresistance (GMR) of the spin valve allows for reading out the state of the spin-orbit torque device^{8,9}.

In a spin valve, the spin-orbit torque per unit moment scales inversely with the free-layer thickness^{1,2}. Hence, a thinner free layer is necessary to enhance the driving efficiency of the device. However, a thinner magnetic layer exhibits increased spin-flip scattering at surfaces, often compounded by poor film quality, which decreases the current spin polarization^{10–14}. Thus, reducing the free-layer thickness to the low single-digit nm regime decreases the GMR response^{15–21}. Combining the ultrathin layers required for efficient torque with robust GMR readout remains a key obstacle.

Here, we demonstrate a strategy to enable strong GMR in spin valves with ultrathin ($\lesssim 2$ nm) free layers. Specifically, introducing a 1-nm Cu seed layer promotes sharp interfaces and pronounced texturing in the free layer, resulting in GMR ratios of $\approx 5 – 7\%$. These values are comparable to conventional spin valves with thicker free layers ($\gtrsim 5$ nm)^{21–24} and far exceed the ratios of $\approx 1\text{--}2\%$ previously reported with ultrathin free layers^{21,25,26}. Our findings present an effective approach toward robust GMR reading for next-generation spin-orbit-torque memories and neuromorphic computers.

All film stacks were grown on thermally oxidized Si substrates (with 50-nm-thick SiO_2) by DC magnetron sputtering; key deposition parameters are listed in the Supplemental Material. Throughout this Letter, we compare ferromagnetic Co-based film stacks grown on two types of seed layers:

- (i) 3-nm Ti (substrate/Ti/Co...) and
- (ii) 3-nm-Ti/1-nm Cu (substrate/Ti/Cu/Co...).

As we systematically show below, the thin Cu seed layer has a profound impact on the structure and performance of the spin valve. Ti was selected for ensuring good adhesion between the oxide substrate surface and the subsequent metal layers. Co was selected because it is among the highest-GMR ferromagnetic metals that are commonly used. All measurements were performed in ambient air at room temperature.

To determine the quality of the interface between the seed layer and the subsequent Co layer, we conducted X-ray reflectivity (XRR) on Ti- and Ti/Cu-seeded Co films, each 30 nm thick and capped with 3-nm Ti for protection against oxidation. Figure 1(a) shows the XRR data, along with modeled curves produced with GenX²⁷ to quantify the interfacial width σ (i.e., diffuseness or roughness). The XRR intensity for Ti-seeded Co decays sharply at higher angles. This decay corresponds to a broad interfacial width of $\sigma \approx 1.1$ nm at the bottom Ti/Co interface, likely due to Ti-Co intermixing. By comparison, the XRR intensity for Ti/Cu-seeded Co decays much more gradually, indicating a sharp Cu/Co interface with $\sigma < 0.3$ nm. Moreover, the XRR results reveal a more diffuse or rougher top Co interface for the Ti-seeded case ($\sigma \approx 1.5$ nm) than the Ti/Cu-seeded case ($\sigma \approx 1.0$ nm). Overall, we find that the ultrathin Cu seed layer yields sharper Co interfaces.

In addition to interfacial sharpness, we also anticipate the Cu seed layer to stabilize FCC (111) out-of-plane crystal orientation (texture)^{28–30} of the subsequent polycrystalline Co-based spin valve. To verify such Cu-aided texturing, we compare $2\theta\text{-}\omega$ X-ray diffraction (XRD) of Ti- and Ti/Cu-seeded Co/Cu/Co spin-valve-like stacks, each capped with Ti. Figure 1(b) shows XRD results for stacks with 3.0-nm Co layers and a 3.5-nm Cu spacer. The Ti-seeded stack shows only a small diffraction peak centered around $2\theta \approx 44^\circ$. No significant out-of-plane texturing is evidenced for Co; the small diffraction peak is attributed to the weak (111)

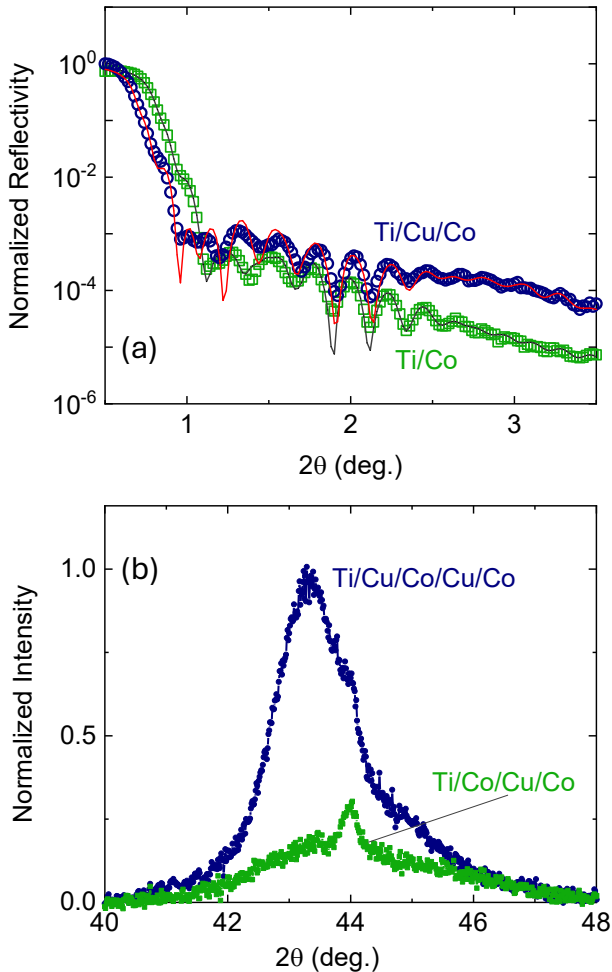


FIG. 1. (a) XRR data (symbols) and fits (solid curves) for Ti- and Ti/Cu-seeded Co(30 nm) films. The fits were used to extract the interfacial width σ (diffuseness or roughness). (b) XRD of Ti- and Ti/Cu-seeded Co(3.0 nm)/Cu(3.5 nm)/Co(3.0 nm) stacks.

texturing of the Cu spacer, as identical XRD is obtained from a control 3.5-nm Cu film sandwiched between 3-nm Ti, as shown in Supplementary Material. In contrast, the Ti/Cu-seeded stack exhibits a markedly taller FCC (111) diffraction peak. This finding indicates that the ultrathin Cu seed layer strongly promotes (111)-oriented growth of the subsequent FCC metal layers –i.e., not only Cu but also Co.

We now proceed to address the crucial question: how does the distinct structural quality resulting from Ti and Ti/Cu seed layers impact the conductance and GMR of spin valves? Hereafter, each spin valve consists of a Co free layer of variable thickness, a 3.5-nm nonmagnetic Cu spacer layer, a 3.0-nm Co fixed layer, a 7-nm antiferromagnetic $\text{Fe}_{50}\text{Mn}_{50}$ exchange-biasing layer, and a 1-nm Cu/3-nm Ti capping layer. To establish the exchange-bias direction, each spin valve was grown under an in-situ forming field of 28 mT from a pair of Alnico

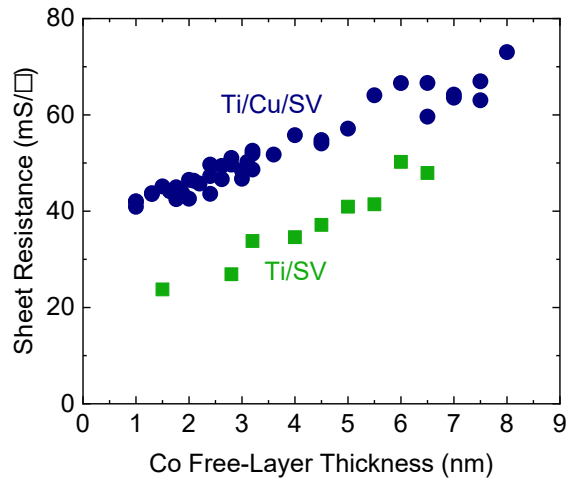


FIG. 2. Sheet conductance for Ti/SV and Ti/Cu/SV plotted against the Co free-layer thickness.

permanent magnets. We denote a Ti-seeded spin valve as “Ti/SV” and Ti/Cu-seeded spin valve as “Ti/Cu/SV.”

Figure 2 compares the sheet conductance, measured with the standard van der Pauw method, of the Ti/SV and Ti/Cu/SV series plotted against Co free-layer thickness. Ti/Cu/SV shows a systematically higher sheet conductance compared to Ti/SV by almost a factor of 2 in the ultrathin regime. One might expect Ti/Cu/SV to be more conductive simply because the 1-nm Cu seed layer provides an additional conductive path. However, separate measurements reveal that the conductance of 1-nm-thick Cu (sandwiched between 3-nm Ti layers) only has a sheet conductance of $< 3 \text{ mS}/\square$. Therefore, the $\approx 20 \text{ mS}/\square$ higher sheet conductance of Ti/Cu/SV requires another explanation.

A plausible possibility is that the superior crystalline and interfacial quality of Ti/Cu/SV leads to higher conductance than Ti/SV. In particular, the textured, sharp interfaces in Ti/Cu/SV likely favor specular electron scattering (preserving momentum) over diffuse scattering (destroying momentum) at the interfaces. From a practical perspective, the higher sheet conductance is beneficial for reducing power dissipation in the spin valve. Moreover, with the minimal current shunt through the Cu seed layer, a substantial fraction of the in-plane current can flow through the ferromagnetic layers, permitting robust GMR as we show in the following.

To characterize GMR, we measured the sheet resistance under a sweeping in-plane magnetic field applied along the exchange-bias axis. Figure 3(a,b) shows examples of how the normalized sheet resistance evolves with the magnetic field. The hysteresis loop seen in each case captures the switching of the free layer. In particular, the lower resistance level R_{\min} indicates that the free-layer magnetization is parallel to the fixed-layer magnetization, whereas the higher resistance R_{\max}

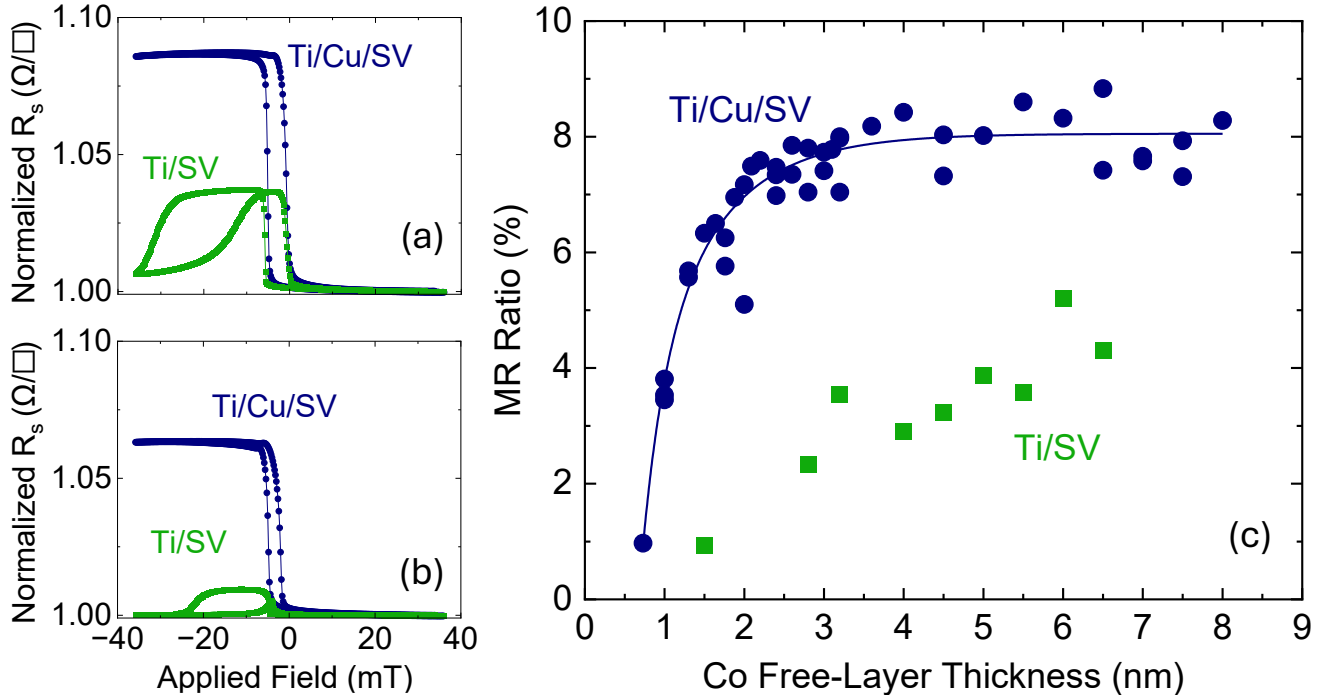


FIG. 3. (a,b) Representative GMR curves from the Ti/SV and Ti/Cu/SV series with free-layer thicknesses of (a) 5.5 nm and (b) 1.5 nm. (c) GMR ratio as a function of Co free-layer thickness for Ti/SV and Ti/Cu/SV.

indicates that the free-layer magnetization is antiparallel to the fixed-layer magnetization. We quantify the GMR ratio as

$$MR = \frac{R_{\max} - R_{\min}}{R_{\min}}. \quad (1)$$

At the Co free-layer thickness of 5.5 nm, $MR \approx 8\%$ for Ti/Cu/SV is about a factor of 2 greater than $MR \approx 4\%$ for Ti/SV [Fig. 3(a)]. With the free-layer thickness reduced to 1.5 nm, this difference increases to about a factor of 6, as Ti/Cu/SV maintains a high GMR ratio of $MR \approx 6\%$ while Ti/SV shows a deteriorated ratio of only $MR \approx 1\%$ [Fig. 3(b)]. We also observe that in the Ti/SV samples, the resistance reverts to R_{\min} even under a modest negative applied field, indicating that the fixed-layer magnetization readily flips. Indeed, our static magnetometry results, shown in the Supplementary Material, confirm that exchange-bias pinning is weak in the fixed layer of Ti/SV. The weak exchange bias is consistent with the limited crystal texturing of Ti/SV, since exchange bias in FCC systems is known to be correlated with (111) texturing^{31,32}. The lack of crystal texture in the bottom Co free layer of Ti/SV propagates through the stack, producing poor texturing in the top Co fixed layer that weakens the exchange bias.

Figure 3(c) further highlights the superiority of Ti/Cu/SV over Ti/SV, especially at smaller free-layer thicknesses. In the Ti/SV series, the GMR ratio dips to $MR < 2\%$ at 3 nm of free-layer thickness and essentially vanishes below 2 nm – similar to conventional

spin valves from earlier experiments^{21,25,26}. In contrast, the GMR ratio of the Ti/Cu/SV series remains close to the saturated value down to a free-layer thickness of around 2 nm. Even in the free-layer thickness window of 1.3 – 2 nm, we still observe high GMR ratios of $MR \approx 5\text{--}7\%$. We emphasize that the high GMR ratios of our ultrathin-free-layer spin valves are on par with those with a considerably thicker free layer (≈ 5 nm)^{21–24}.

The stark contrast in GMR emerges from the different qualities of Ti- and Ti/Cu-seeded Co. The first few atomic monolayers of Co on Ti produce a diffuse Ti/Co interface, causing spin-flip scattering that reduces the GMR ratio in Ti/SV. The Co layer on Ti also develops very little crystal texturing, which may further contribute to the reduced GMR ratio. In contrast, Co growth templated with the Cu seed layer yields a highly textured film with a sharp interface, such that even a $\lesssim 2$ -nm Co free layer can attain bulk-like current spin polarization. The coherent crystal structure plausibly reduces scattering sites or spatial variations in spin-orbit coupling that could otherwise depolarize the current. Thus, the ultrathin Cu seed enables high GMR ratios even for small Co free-layer thicknesses.

Having demonstrated the critical role of the Cu seed layer, we also address the impact of its thickness on GMR. Figure 4 shows the GMR ratio as a function of Cu seed layer thickness, with the Co free-layer thickness fixed at 5 nm and the Cu seed layer varied from 0 to 5 nm. The GMR ratio remains nearly constant for Cu seed layer thicknesses between 1 and 3 nm. This

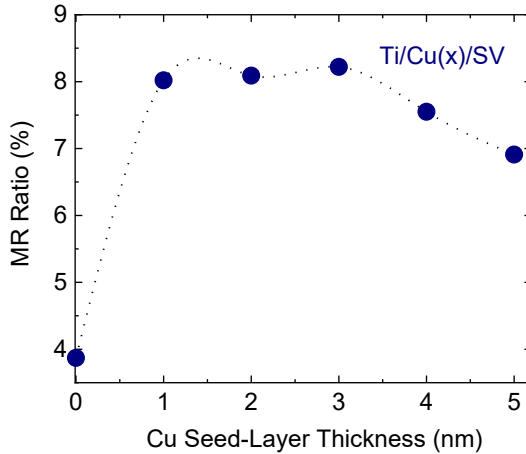


FIG. 4. GMR ratio as a function of Cu seed-layer thickness with a Co free-layer thickness of 5 nm.

observation confirms that just a few atomic monolayers of Cu form an excellent template for the subsequent Co-based spin valve. It also suggests that, within the thickness range of 1 – 3 nm, the seed layer promotes high-quality film growth without significantly modifying the current distribution in the ferromagnetic layers of the spin valve. When the Cu seed layer exceeds about 4 nm, the GMR ratio decreases, which can be attributed to current shunting through the thicker, more conductive Cu layer. In this case, a larger portion of the current bypasses the magnetic layers, reducing the fraction of the spin-polarized electric current and thereby lowering the measured GMR ratio.

In summary, we have investigated current-in-plane spin valves whose free layers are seeded by Ti or Ti/Cu. Our results show that the incorporation of 1-nm Cu significantly improves the structural quality of the magnetic layers, accompanied by high GMR. This effect is especially pronounced for thinner free layers; at free-layer thicknesses of ≈ 1.3 – 2 nm, Cu-seeded spin valves exhibit GMR ratios of ≈ 5 – 7%, in contrast to vanishing GMR for spin valves lacking a Cu seed. The high GMR ratios with such thin free layers are particularly attractive for spin-orbit-torque applications of spin valves. Our approach offers a scalable, effective pathway to high-signal GMR readout for emerging spintronic memories and neuromorphic computers.

ACKNOWLEDGMENTS

S.A. and S.E. were supported by the National Science Foundation (NSF) under Grant No. ECCS-2236160. R.E.M. was supported by the National Science Foundation (NSF) under Grant No. DMR-2144333. This research used resources in the Structural Characterization Lab in the Department of Materials Science and Engineering at Virginia Tech.

DATA AVAILABILITY

The data that support the findings of this study are available from the corresponding authors upon reasonable request.

- ¹A. Manchon, J. Železný, I. M. Miron, T. Jungwirth, J. Sinova, A. Thiaville, K. Garello, and P. Gambardella, *Rev. Mod. Phys.* **91**, 035004 (2019).
- ²Q. Shao, P. Li, L. Liu, H. Yang, S. Fukami, A. Razavi, H. Wu, K. Wang, F. Freimuth, Y. Mokrousov, M. D. Stiles, S. Emori, A. Hoffmann, J. Åkerman, K. Roy, J.-P. Wang, S.-H. Yang, K. Garello, and W. Zhang, *IEEE Transactions on Magnetics* **57**, 1 (2021).
- ³A. Davidson, V. P. Amin, W. S. Aljuaid, P. M. Haney, and X. Fan, *Physics Letters A* **384**, 126228 (2020).
- ⁴K. W. Kim, B. G. Park, and K. J. Lee, *npj Spintronics* **2**, Article 8 (2024).
- ⁵S.-h. C. Baek, V. P. Amin, Y.-W. Oh, G. Go, S.-J. Lee, G.-H. Lee, K.-J. Kim, M. D. Stiles, B.-G. Park, and K.-J. Lee, *Nature Materials* **17**, 509 (2018).
- ⁶D. Kubler, D. A. Smith, T. Nguyen, F. Ramos-Diaz, S. Emori, and V. P. Amin, *Phys. Rev. B* **111**, 054425 (2025).
- ⁷J. Grollier, D. Querlioz, K. Y. Camsari, K. Everschor-Sitte, S. Fukami, and M. D. Stiles, *Nature Electronics* **3**, 360 (2020).
- ⁸J.-R. Chen, A. Smith, E. A. Montoya, J. G. Lu, and I. N. Krivorotov, *Communications Physics* **3**, 187 (2020).
- ⁹Y. Liu, I. Barsukov, Y. Barlas, I. N. Krivorotov, and R. K. Lake, *Applied Physics Letters* **116**, 132409 (2020).
- ¹⁰J. Bass and W. P. Pratt, *Journal of Physics: Condensed Matter* **19**, 183201 (2007).
- ¹¹M. Haidar and M. Bailleul, *Physical Review B* **88**, 054417 (2013).
- ¹²M. Erekhinsky, A. Sharoni, F. Casanova, and I. K. Schuller, *Applied Physics Letters* **96**, 022513 (2010).
- ¹³D. Alcer and D. Atkinson, *Nanotechnology* **28**, 375703 (2017).
- ¹⁴M. Cormier, A. Mougin, J. Ferré, A. Thiaville, N. Charpentier, F. Piéchon, R. Weil, V. Baltz, and B. Rodmacq, *Physical Review B* **81**, 024407 (2010).
- ¹⁵P. Khunkitti, A. Siriratatiwat, and K. Pituso, *Micromachines* **12** (2021), 10.3390/mi12091010.
- ¹⁶B. Elsafi, *ECS Journal of Solid State Science and Technology* **14**, 073002 (2025).
- ¹⁷S. S. P. Parkin, N. More, and K. P. Roche, *Phys. Rev. Lett.* **64**, 2304 (1990).
- ¹⁸I. Bakonyi, E. Simon, B. G. Tóth, L. Péter, and L. F. Kiss, *Phys. Rev. B* **79**, 174421 (2009).
- ¹⁹S. S. P. Parkin, N. More, and K. P. Roche, *Physical Review Letters* **64**, 2304 (1990).
- ²⁰S. Zsurzsa, M. El-Tahawy, L. Péter, L. F. Kiss, J. Gubicza, G. Molnár, and I. Bakonyi, *Nanomaterials* **12**, 4276 (2022).
- ²¹B. Diény, V. S. Speriosu, S. Metin, S. S. P. Parkin, B. A. Gurney, P. Baumgart, and D. R. Wilhoit, *Journal of Applied Physics* **69**, 4774 (1991).
- ²²V. V. Ustinov, M. A. Milyaev, L. I. Naumova, V. V. Proglyado, and T. P. Krinitzina, in *NSTI-Nanotech 2012 Conference Proceedings* (TechConnect Briefs, 2012) paper No. 581.
- ²³S. S. P. Parkin, *Physical Review Letters* **71**, 1641 (1993).
- ²⁴S. N. Kim, J. W. Choi, and S. H. Lim, *Scientific Reports* **9** (2019), 10.1038/s41598-018-38269-w.
- ²⁵P. H. Chan, X. Li, and P. W. T. Pong, *Vacuum* **140**, 111 (2017).
- ²⁶M. Romera, M. Muñoz, P. Sánchez, and C. Aroca, *Journal of Applied Physics* **106** (2009), 10.1063/1.3173580.
- ²⁷M. Björck and G. Andersson, *Journal of Applied Crystallography* **40**, 1174 (2007).
- ²⁸C.-M. Liu, H.-W. Lin, C.-L. Lu, and C. Chen, *Scientific Reports* **4**, 6123 (2014).
- ²⁹D. E. Joyce, C. A. Faunce, P. J. Grundy, B. D. Fulthorpe, T. P. A. Hase, I. Pape, and B. K. Tanner, *Physical Review B* **58**, 5594 (1998).

³⁰C. E. Murray, K. P. Rodbell, and P. M. Vereecken, *Thin Solid Films* **503**, 207 (2006).
³¹G. Choe and S. Gupta, *Applied Physics Letters* **70**, 1766 (1997).

³²I. L. Castro, V. P. Nascimento, E. C. Passamani, A. Y. Takeuchi, C. Larica, M. Tafur, and F. Pelegrini, *Journal of Applied Physics* **113**, 203903 (2013).